Eur. Phys. J. D **7**, 55–64 (1999)

THE EUROPEAN PHYSICAL JOURNAL D

EDP Sciences

Dissociative attachment of low-energy electrons to vibrationally excited Na_2 molecules using a photoelectron source

M. Keil[1], T. Kolling[1], K. Bergmann[1,a], and W. Meyer[2]

[1] Fachbereich Physik der Universität Kaiserslautern, Postfach 3049, 67653 Kaiserslautern, Germany
[2] Fachbereich Chemie der Universität Kaiserslautern, Postfach 3049, 67653 Kaiserslautern, Germany

Received: 21 November 1998 / Received in final form: 7 April 1999

Abstract. The process of dissociative attachment (DA) of low-energy electrons ($0 \leq \varepsilon \leq 40$ meV) to vibrationally excited sodium dimer molecules is studied with high electron energy resolution ($\Delta\varepsilon \approx 2$ meV) in a supersonic molecular beam. A novel photoelectron source, based on two-step photoionization of the sodium atoms in the beam, may deliver a current of up to 1 nA and has been used with a current of typically 0.2 nA in this experiment. The energy dependence of the rate of sodium anion formation is determined by ion detection based on a time-of-flight analysis. The molecules are selectively excited to levels $11 \leq v'' \leq 22$ using the technique of coherent population transfer by delayed pulses (STIRAP). The comparison of the experimental data with recent resonance model calculations based on improved potential curves reveals generally good agreement for levels $v'' > 12$. For $v'' \leq 12$ some distinct differences between theoretical and experimental results persist.

PACS. 34.80.Ht Dissociation and dissociative attachment by electron impact – 34.80.Qb Laser-modified scattering – 31.25.Nj Electron-correlation calculations for diatomic molecules

1 Introduction

Dissociative electron attachment (DA), which results in the formation of negative ions following electron capture by a neutral molecule:

$$e^-(\varepsilon) + AB(v'') \rightarrow AB^{-*} \rightarrow A + B^-,$$

is an important elementary process in plasma physics [1–4]. It is known that the rate of formation of negative ions may vary dramatically with vibrational excitation of the molecule prior to the process of electron capture [5,6]. Experimental observations for ro-vibrationally excited diatomic [5,7–20], as well as polyatomic molecules [20–41] have been made. The high sensitivity of DA to vibrational excitation is understood theoretically in the local complex potential model (also called resonance model) [6,42–50] as well as in non-local models [51–56] or in a classical approach [57].

The DA process is initiated by the capture of an electron e^- with an energy ε into a molecular orbital which is often associated with a repulsive intramolecular potential of the negative complex (which is the case for sodium molecules, see Fig. 1), causing the atoms to separate. If the electron is reemitted before the atoms have separated far enough to form a stable atomic anion, the neutral molecule is usually left in a vibrationally excited state v''_f after the process. Ion formation by DA depends on a sufficiently long-resonance lifetime. Specifically, the bond distance R must increase to the region $R > R_S$, where $V^-(R) < V(R)$. In the case of sodium $V^-(R)$ is the interaction potential $A^2\Sigma_g$ between the negative atomic ion and the rest of the molecule, while $V(R)$ describes the neutral particle interaction potential $X^1\Sigma_g$ with a free non-interacting zero-energy electron. The crossing of $V^-(R)$ and $V(R)$ occurs at $R = R_S$.

In the past, most experiments aiming at the characterization of the vibrational dependence of the DA process relied on thermal excitation of the molecule. Optical methods [9,10,17,58] as well as other approaches [18] have also been used. These methods do not allow selective population of excited states.

Here, we expand on our previous work [9,10] using the technique of coherent population transfer (STIRAP) for efficient and selective population of vibrational levels [59–62]. Following the pioneering work of Ziesel *et al.* [63], who observed the Na^- formation from DA to Na_2 in an effusive molecular beam, we demonstrated the dramatic variation of the rate of negative ion formation with vibrational excitation of the $Na_2(v'')$ molecules in the range $0 \leq v'' \leq 25$ [10]. While that work was performed with a conventional electron source with low-energy resolution, we use here a novel type of high-energy resolution and high-current photoelectron source. Such an experiment, combining selective vibrational excitation with high elec-

[a] e-mail: bergmann@rhrk.uni-kl.de

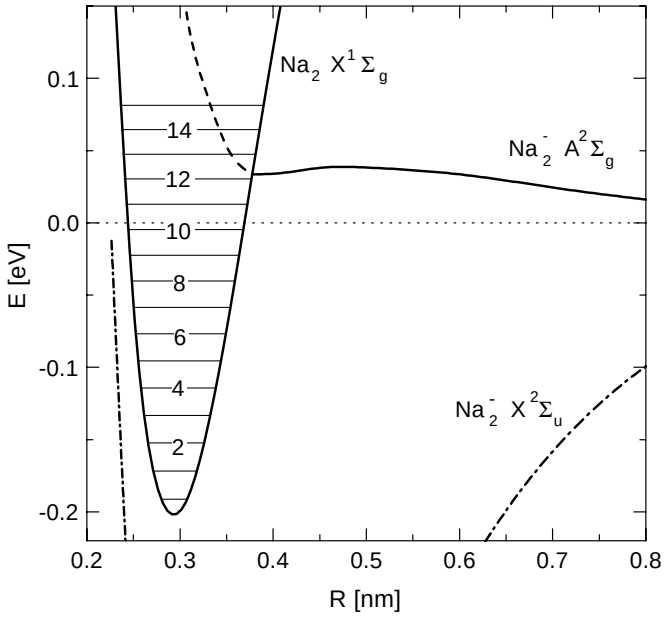

Fig. 1. Details of the potential curves $X^1\Sigma_g^+$ for the neutral Na_2 molecule and the molecular negative ion Na_2^- ($A^2\Sigma_g^+$) near the crossing point at R_S. Results obtained from the new MR-CI calculations are shown, using an expanded basis as compared to those results reported in reference [10]. For large distances, the negative ion curve reaches the energy indicated by the horizontal dotted line. The energies of the vibrational states of the neutral molecule are also shown.

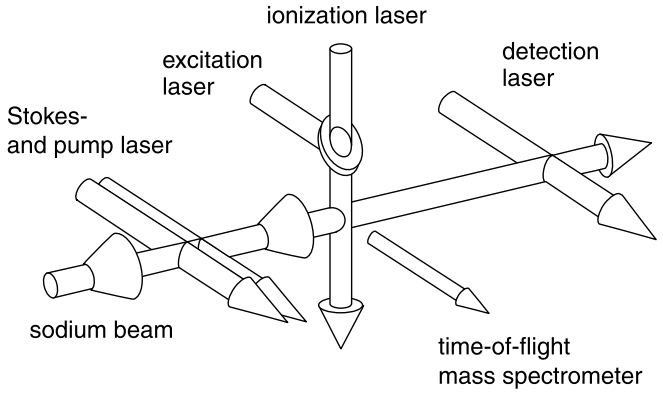

Fig. 2. Experimental setup: the sodium molecules travelling in a collimated supersonic beam first cross two single-mode lasers, the Stokes and the pump laser with their axes slightly displaced. These two lasers induce the vibrational excitation of the molecules. Behind a second collimation, the excitation and ionization lasers intersect the particle beam and produce electrons by two-step ionization of sodium atoms. Negative ions formed by DA in this region are accelerated into a 20 cm long Wiley-McLaren-type time-of-flight mass spectrometer. A fifth laser further downstream probes the efficiency of the vibrational state preparation by laser-induced fluorescence.

tron energy resolution, carries the potential to reveal interesting and important features of the DA process, such as the relevance of non-local interaction. This is true, in particular, if the molecule is excited to vibrational levels which allow the capture of a very low-energy electron at bond distances near R_S.

The electronic configuration of the $X^2\Sigma_u^+$ ground state of the molecular negative ion Na_2^- is $1\sigma_g^2 1\sigma_u$. This lowest-lying state of the molecular negative ion is stable (unlike for H_2 [64]) and is not involved in the processes of interest here. Its minimum lies 0.443 eV below the minimum of the ground state $X^1\Sigma_g^+$ of the neutral molecule (see Sect. 6.2). The $A^2\Sigma_g^+$ state is stable for $R \geq 0.38$ nm and turns into a resonance state for smaller R. At long range it is dominated by the $1\sigma_g 1\sigma_u^2$ configuration. It acquires significant admixture of a $1\sigma_g^2 2\sigma_g$ configuration at distances below 0.5 nm. For $R \leq R_S$ the orbital $2\sigma_g$ turns into a continuum wave function, *i.e.* the capture process places an electron into a $1\sigma_u$ orbital while, at the same time, a valence electron is promoted from the $1\sigma_g$ to the $1\sigma_u$ orbital.

An early discussion of the relevant potential curves can be found in [65–67]. A more recent detailed characterization of the orbitals supporting the resonance is given in reference [10] with additional comments provided in Section 4 of this paper.

2 The experimental setup

The experimental setup is schematically shown in Figure 2. We use a differentially pumped vacuum system with three chambers which contain a sodium beam source, a region for vibrational excitation of the molecules by coherent population transfer (see Sect. 5), a scattering region with the integrated photoelectron source (see Sect. 3) as well as an ion detector, which terminates a time-of-flight section for mass analysis, and a monitor based on laser-induced fluorescence.

The sodium beam source is operated at 900 K with the nozzle being held 50 K hotter. The corresponding sodium vapor pressure is approximately 50 mbar. The resulting supersonic expansion through the 0.4 mm diameter nozzle hole produces a particle beam with a Na_2 mole fraction of the order of 15%. Most of the molecules (99%) are found in the ground vibrational level [68]. The population of rotational levels for $j'' < 15$ is best characterized by $T_{\rm rot} = 27 \pm 10$ K [10], meaning that about 8% of all the molecules are found in the rotational level $j'' = 9$ which is used in this experiment. A pair of heated skimmers in combination with the 3 mm diameter aperture at the entrance to the scattering region form a well-collimated beam with a divergence angle of less than 1°.

After being vibrationally excited by the combined interaction of two laser beams with the molecules [59–62], the sodium beam is intersected further downstream (in the center of the scattering region) by two more laser beams. These lasers create the photoelectrons by two-step photoionization of sodium atoms which are abundant in the sodium beam. An acousto-optical modulator is used to switch on the continuous laser, which pumps the population to the $3p$ state, for 1 μs. An extraction pulse of

1 μs duration is applied with a delay of 0.2 μs. The negative ions formed by the DA process are accelerated into a 20 cm long Wiley-McLaren-type time-of-flight mass spectrometer and detected by a stack of three multichannel plates. Finally, a fifth laser beam crosses the molecular beam downstream of the scattering region and monitors the efficiency of the vibrational excitation process.

3 The electron source

In this section we first discuss the basic features of the photoelectron source and then comment on the influence of a small magnetic field on the effective current before discussing the various contributions to the width of the collision energy distribution of the electrons.

3.1 The photoelectron current

Since the pioneering work of Gallagher and coworkers [69], only few applications of photoelectron sources to collision dynamics studies have been reported, see, *e.g.*, Field *et al.* [70,71] and Chutjian and coworkers [72,73]. In particular noteworthy is the work of Hotop and coworkers [74, 75] who have demonstrated an energy resolution of the order of 0.05 meV, based on the two-step photoionization of rare-gas atoms by continuous lasers out of one of their metastable states [76].

In the present experiment, the electrons are produced by two-step photoionization of sodium atoms copropagating with the molecules in the beam. The relevant level scheme is shown in Figure 3. The atoms are first excited from the ground state to the 3*p*-level with radiation from a single-mode cw-dye laser ($\lambda_{ex} = 589.158$ nm, $P_{ex} < 100$ mW) and then ionized by the light of a frequency-doubled mode-locked titanium: sapphire laser ($\lambda_{ion} < 408.562$ nm) with a power of about 400 mW. The energy of the electrons is determined by the frequency of the ionization laser. The pulses of that laser, with a pulse width of about 2 ps, are delivered with an efficiency of about 50% through a VIS/UV multi-mode quarz-quarz fiber to the scattering apparatus at a repetition rate of 76 MHz. During the 13 ns between pulses the atoms move only a distance of the order of μm. Therefore, each atom is exposed to the order of 100 pulses. With an average power of the ionization laser of $P_{ion} = 400$ mW, an electron current of 1 nA is observed. However, in order to reduce the broadening of the photoelectron energy distribution because of the build-up of a space charge due to the positive ion cores (see also below), the source is typically operated at an electron current of only 200 pA.

Figure 4 shows the variation of the photoelectron current as a function of the frequency of the continuous laser, which excites the atoms to the 3*p*-level, for a range of 4 GHz near the transition frequency of the sodium *D*2 line. Optical pumping between the hyperfine levels needs to be considered to understand the spectrum. When the laser is tuned to the $F = 2 \rightarrow F' = 3$ or the $F = 1 \rightarrow F' = 0$ transition (separated by 1.713 GHz), excitation seemingly

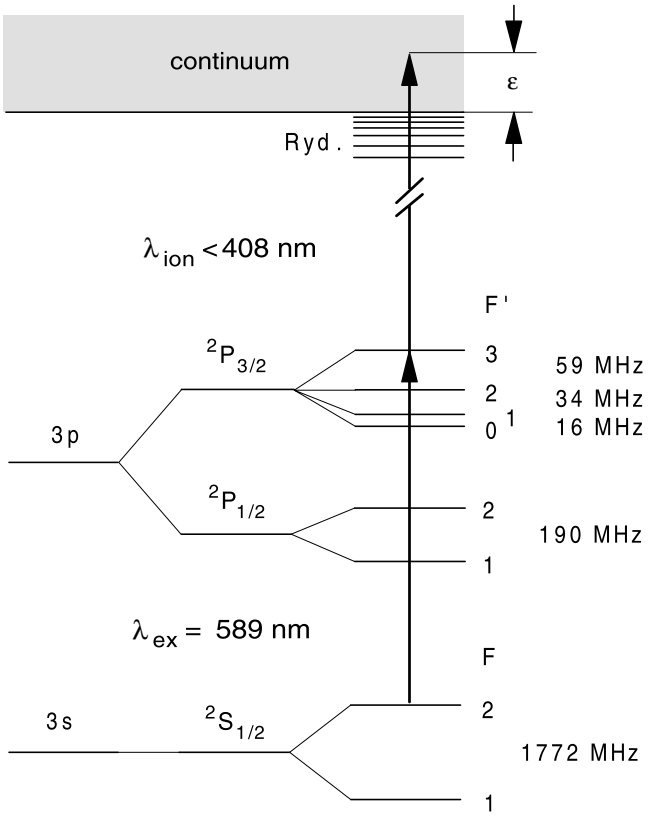

Fig. 3. Level scheme: a single-mode dye laser excites the Na atoms from the $F = 2$ hyperfine level of the electronic ground state $3s\ ^2S_{1/2}$ predominantly to the $F = 3$ level of the $3p\ ^2P_{3/2}$ state. The excited atoms are ionized by a train of pulses from a frequency-doubled mode-locked titanium: sapphire laser.

occurs in a closed two-level system. In that case radiative decay from the excited state is restricted by optical selection rules to emission back to the initial level. However, even for such tuning, neighboring hyperfine levels in the 3*p* states are also weakly excited through the wings of the spectral profile of the laser, leading to the loss of atoms by decay to the other (not excited) hyperfine level in the ground state. This loss is severe, when the excitation occurs to levels $F' < 3$ starting at $F = 2$ or to $F' > 0$ starting at $F = 1$ since the interaction time of the laser with atoms is much longer than the 16.3 ns [77] lifetime of the Na $3p\ ^2P_{3/2}$ state. The electron current is highest, when the laser frequency is tuned close to the $F = 2 \rightarrow F' = 3$ transition frequency, since the loss due to optical pumping is smallest in this case.

The small structure between the peaks related to the transitions discussed above (see in Fig. 4) is found when the (small) far wing excitation probability out of the $F = 1$ and the $F = 2$ state are equal. In that case, nearly complete loss of the population to the other hyperfine level is not possible and some atoms are excited to the 3*p* state, even in the steady-state limit.

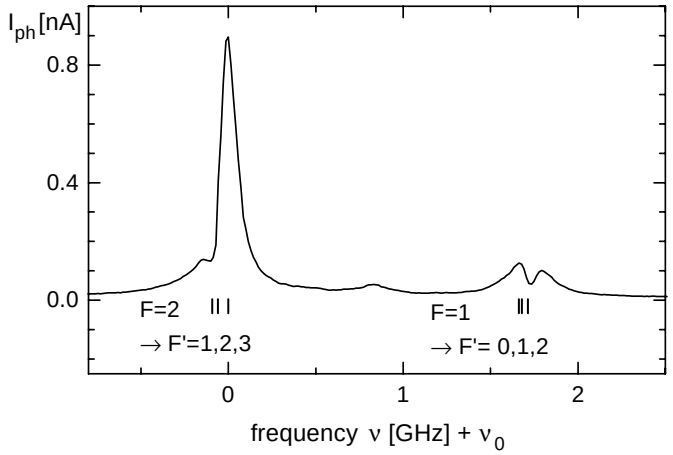

Fig. 4. The variation of the photoelectron current with the frequency of the excitation laser: the structure near the frequencies labeled zero and 1.7 GHz are related to excitation out of the $F = 2$ and $F = 1$ hyperfine levels of the ground state, respectively. Intensities are strongly determined by optical pumping processes. The nature of the little peak halfway between the main structure is explained in Section 3.

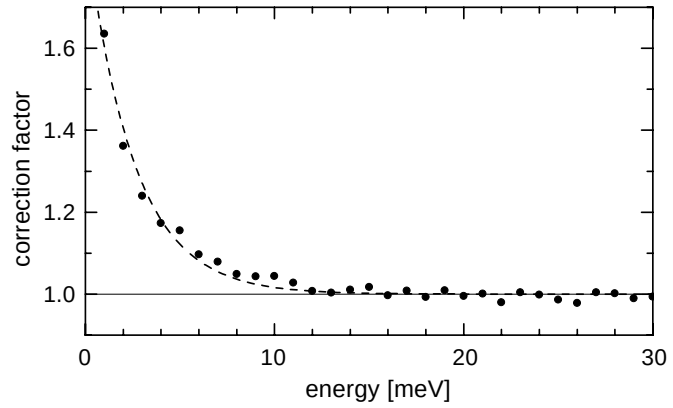

Fig. 5. Correction factor due to the cyclotron motion of the electrons in the residual magnetic field, needed to convert the measured photoelectron current into an effective one. The factor remains unity for energies > 30 meV.

3.2 The energy dependence of the effective photoelectron current

In Section 4 we discuss the electron energy dependence of the rate of negative ion formation. It is crucial to establish the dependence of the effective photoelectron current on energy. We typically cover a range of less than $\varepsilon = 100$ meV. The variation of the photoionization cross-section over this range is small [78] and can be accounted for. However, cyclotron motion of the electrons in the residual magnetic field may lead the electrons back into the scattering region, thus increasing the effective photoelectron current in particular for very low-energy electrons.

We have determined the related enhancement factor by simulation studies in the following way. The starting points of the electrons were chosen at random within the scattering region, assumed to be spherically symmetric. At each starting point, the emission angle with respect to the magnetic-field direction is also chosen at random. The direction of the residual magnetic field, measured to be of the order of 1 G, is perpendicular to the molecular beam axis, since it stems mainly from the magnetic field used in the time-of-flight section to prevent electrons from reaching the detector [10]. The trajectory of each electron, which generally has the form of a spiral around the magnetic-field direction, is followed and the path length within the scattering region determined. When the electron hits anyone of the walls near the scattering region, the trajectory is terminated. When the electron has not returned to the scattering region after the completion of a full cycle of the cyclotron motion, the trajectory is also terminated. Some trajectories do lead the electrons back to the scattering region. In that case, the path length through that region is added to the previous one and a correction factor is determined accordingly. Obviously, the chance for returning to the scattering region due to the cyclotron motion increases with decreasing electron energy. Figure 5 shows the energy dependence of the correction factor which needs to be applied to determine the effective photoelectron current. The correction factor deviates substantially (more than 10%) from unity only for electron energies smaller than 5 meV (see Fig. 5). In conclusion, we emphasize that the residual magnetic field has no influence on the effective photoelectron current for electron energies > 10 meV.

3.3 The photoelectron energy resolution

The energy resolution of the photoelectron source is determined by several factors [69,79]. Those which are most important in our experiment are described in the following.

(a) The energy spread related to the transform limited bandwidth of the radiation of the ionization laser provides a lower limit to the attainable electron energy resolution. Since the light pulses are obtained by mode locking, their bandwidth is nearly Fourier limited with a time-bandwidth-product of $\Delta t \Delta \nu \approx 0.5$. The pulse width is $\Delta t = 2$ ps. Therefore, the contribution to the energy spread is approximately

$$\Delta E_{(a)} = h/2\Delta t \leq 1 \text{ meV}\,.$$

with the distribution function being nearly Gaussian. Here and below ΔE measures the full width half maximum (FWHM).

(b) The space charge established by the ionized Na^+ atoms is another significant cause for a spread of the energy of the electrons. After ionization the photoelectrons quickly leave the scattering region, while the Na^+ ions stay behind, forming a region of positive space charge. The energy of the electrons is therefore not only determined by the excess of the photon energy over the ionization energy, but depends also on the location within the space charge

region, where ionization occurs. A precise determination of the electron energy distribution requires a detailed numerical analysis, taking into account the exact location of the individual photoionization process and the exact location of the collision, possibly also considering the discrete distribution of the positive ions [80].

Here, an estimate based on the following simplication suffices. We assume a spherically symmetric region of homogeneously distributed positive charges. The potential inside this sphere is $\phi(r) = \rho r^2/(3\epsilon_0)$. The charge density ρ is related to the current $I_{\rm ion}$ of the positive ions. Since this current is equal to the electron current $I_{\rm ph}$, we have $\rho = I_{\rm ph}/(\overline{v}\rho R^2)$, where $\overline{v}$ is the mean velocity of the positive ions and R is the diameter of the ion cloud. The maximum potential difference $\Delta\phi_{\rm max}$ occurs between the center of the space charge region ($r = 0$) and its boundary ($r = R$). With $\Delta\phi_{\rm max} = \phi(r = R) - \phi(r = 0) = I_{\rm ph}/(3\pi\epsilon_0\overline{v})$ we find the upper limit of the space charge related energy spread to be $\Delta E_{(b)}^{\rm max} = 2eI_{\rm ph}/(3\pi\epsilon_0\overline{v})$. The factor of 2 is applied for this estimate since electrons may gain or lose energy, depending on whether they are born near the boundary and collide with a molecule near the center of the space charge region or *vice versa*. Both numerical simulation studies as well as analytical calculations [79] show that the energy distribution function is of triangular shape with a width (FWHM) of $\Delta E_{(b)} \leq \Delta E_{(b)}^{\rm max}/2 = eI_{\rm ph}/(3\pi\epsilon_0\overline{v})$. The mean velocity of the positive ions is equal to the mean velocity of the neutral atoms traveling in the beam. With $\overline{v} = 1340$ m/s we find

$$\Delta E_{(b)}\ [\text{meV}] \leq 7.5 \times I_{\rm ph}\ [\text{nA}].$$

Under typical operating conditions ($I_{\rm ph} = 200$ pA) we have $\Delta E_{(b)} \leq 1.5$ meV.

(c) The angular distribution of the photoelectron emission contributes to the energy spread of the collision energy, if there is a significant velocity slip Δv between the atoms and the target molecules. The collision energy, in the laboratory frame, depends on the emission angle ϑ of the electrons with respect to the molecular beam axis,

$$E_{\rm lab} = \frac{1}{2}m_e v_e'^2 = \frac{1}{2}m_e(v_e^2 + 2\Delta v v_e\cos\vartheta + \Delta v^2)\,,$$

where v_e is the center-of-mass (sodium ion-electron) velocity determined by the ionization wavelength $\lambda_{\rm ion}$ and the ionization wavelength at the threshold $\lambda_{\rm thr} = 408.562$ nm

$$E_{\rm CM} = \frac{1}{2}m_e v_e^2 = hc\left(\frac{1}{\lambda_{\rm ion}} - \frac{1}{\lambda_{\rm thr}}\right),$$

Since the excitation of the atoms is saturated and the radiation driving the $3s$-$3p$ transition is only weakly polarized the m-levels are equally populated. Therefore, the electron emission is nearly isotropic. The maximum deviation from the mean collision energy (obtained for $\cos\vartheta = 0$) is $\Delta E_{(c)} = m_e v_e \Delta v$. In the case of DA to Na_2 molecules the average velocity slip Δv between the atoms and the target molecules is of the order of 100 m/s. We find

$$\Delta E_{(c)}^{\rm Na_2}\ [\text{meV}] = 0.024 \times \sqrt{\varepsilon\ [\text{meV}]},$$

where ε is the electron energy. In the case of the electron attachment to SF_6 molecules (see Sect. 4), the mean velocity of the static gas is zero. Therefore, the average relative velocity is $\Delta v = 1340$ m/s. The resulting contribution to the energy spread is

$$\Delta E_{(c)}^{\rm SF_6}\ [\text{meV}] = 0.29 \times \sqrt{\varepsilon\ [\text{meV}]}.$$

$\Delta E_{(c)}$ does not exceed 0.2 meV for Na_2 and 2 meV for SF_6, in the range of interest here.

(d) The finite width of the velocity distribution of atoms and molecules in the beam parallel and perpendicular to the molecular beam axis as well as stray electric fields in the scattering region also contribute to the width of the distribution of electron collision energies. However, these latter contributions are neglected here since they are very small compared to those discussed above.

The overall width of the collision energy distribution results from a convolution of all contributions discussed under (a)-(c). The results are confirmed experimentally as discussed in the next Section 4.

4 SF_6 test measurements

The well-studied process (see, *e.g.*, [23,30,81])

$$SF_6 + e^-(\varepsilon) \rightarrow SF_6^-$$

has been chosen as a test case to determine the energy resolution of the photoelectron source. It is known that the attachment rate for free electrons ($\varepsilon > 0$ meV) decreases sharply with increasing electron energy. Klar *et al.* [82] found that the variation of the attachment cross-section with energy closely follows the empirical function (originally proposed by Klots [83])

$$\sigma_e(\varepsilon) = \frac{\sigma_1}{\varepsilon} \times (1 - \exp(-\beta\sqrt{\varepsilon})) \qquad (1)$$

with the parameters $\sigma_1 = 7130 \times 10^{-16}$ cm$^2 \pm 5\%$ and $\beta = 0.405 \pm 10\%$, where ε is in meV.

Results obtained with our photoelectron source are shown in Figure 6. As always, the energy of the electrons is controlled by the frequency of the ionization laser. Below the ionization threshold ($\varepsilon < 0$ meV) $Na^{**}(n,l)$-Rydberg states with l is 0 or 2 and $n > 12$ are excited at specific and well-known photon energies. Charge transfer from these Rydberg states to SF_6 molecules also leads to the formation of negative ions [82]. A sufficiently large number of Rydberg states is observed to allow, by extrapolation, the precise determination of the ionization threshold as well as the calibration of the energy of the free electrons.

The comparison of the variation of the negative ion rate observed in our experiment with the function (1) is shown in Figure 7. Very good agreement is found for energies in the range from 3 meV to 90 meV, using the parameter $\beta = 0.43 \pm 0.03$. At 95 meV an indication of the known [81,84] structure related to the excitation of the symmetric ν_1 stretch vibration is observed. At energies

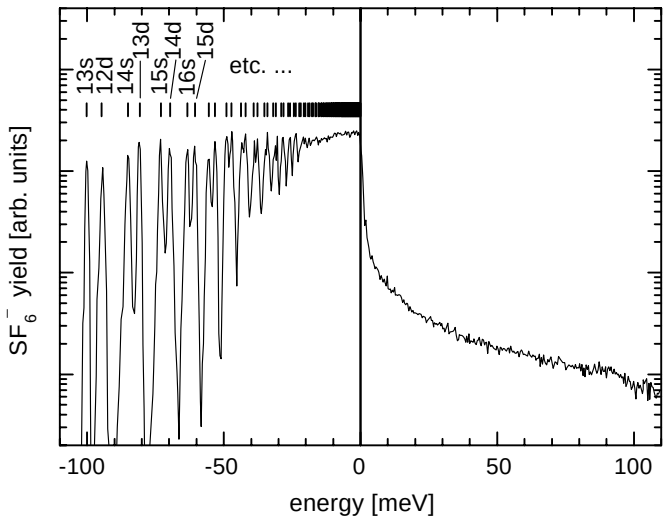

Fig. 6. Electron attachment to SF_6: the SF_6^- yield is shown as a function of the electron energy. Free electron attachment occurs for electron energies $\varepsilon > 0$, while charge transfer out of Rydberg states of Na is observed for $\varepsilon < 0$.

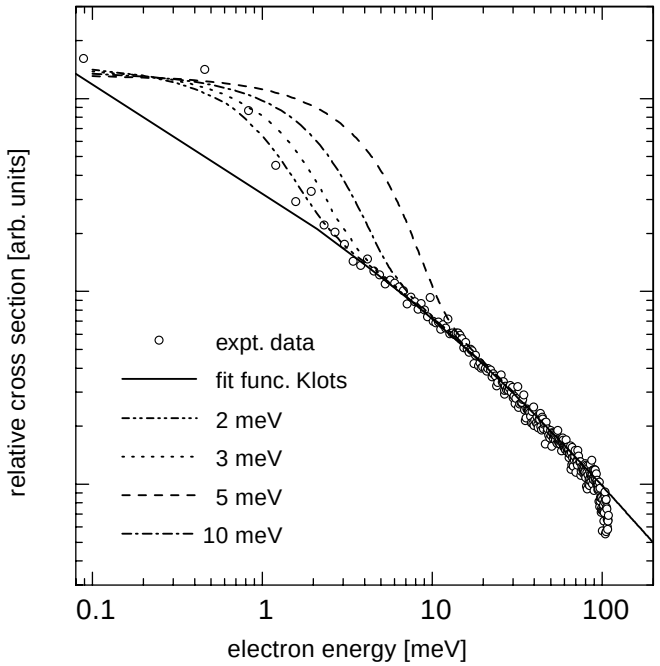

Fig. 7. Comparison of the experimentally observed energy dependence of the relative attachment cross-section to SF_6 with the prediction of the empirical formula equation (1). The latter is folded with a Gaussian distribution function of electron energies with various widths $\Delta\varepsilon$. Best agreement is found for $\Delta\varepsilon = 2$ meV.

below 3 meV the experimental results deviate from the functional form of equation (1) because of the finite energy resolution in our experiment. A reliable estimate of the energy resolution is obtained by convoluting equation (1) with a distribution function (of variable width) for the electron energy, here assumed to be Gaussian. Good agreement between data and fit is found for a width (FWHM) of 2 meV, consistent with the results from Section 3.

5 Molecular state preparation

The significance of the present experiment lies in the combination of a novel high-resolution electron source with an optical method for efficient and selective population of vibrational levels. A review of traditional methods for optical state selection can be found in [85].

For some preliminary experiments, we employed the Franck-Condon pumping (FCP) method [85]. A single laser beam is used to excite molecules from the level $(v'' = 0, j'' = 9)$ of the electronic ground state to a suitably chosen level (v', j') of the electronic A-state, from where they return to the electronic ground state by spontaneous emission. The population distribution is determined by the relevant optical transition rates $R(v'', v')$. For a given level v', populated in the A-state, the population distribution established in the ground state is known [10,86,87]. It can be varied by varying the level v'.

Data with state selectively prepared molecules is obtained by means of the method of coherent population transfer, called STIRAP (stimulated Raman scattering involving adiabatic passage [59]). For a recent review see [60]. Implementation of the STIRAP method for population transfer from a thermally populated level 1 (here the level $v''_i = 0, j''_i = 9$) to a final level (here $v''_f > 0, j''_f = 9$) requires two lasers, a pump laser and a Stokes laser, with both laser frequencies tuned to resonance (or near resonance) with the frequencies for transitions between the initial or final level, respectively, to an intermediate level (here $v', j' = 10$ in the A-state). The laser beams cross the molecular beam at a right angle with their axes shifted spatially. The molecules encounter the Stokes field first and the pump field next (see Fig. 2). The laser beam profiles need to have a suitable overlap. In practice, the Stokes laser frequency is detuned by about 100 MHz from the resonance frequency for transitions from the final level to the intermediate one, with the pump laser frequency detuned from the respective transition accordingly, to maintain the two-photon resonance. When properly implemented, spontaneous emission from the intermediate level does not occur and thus, vibrational levels other than the one for which two-photon resonance is established, do not receive population. In summary, the STIRAP method allows the transfer of all the population of the initial level to the final one.

The transfer efficiency is monitored by fluorescence induced by a probe laser, which crosses the molecular beam downstream of the scattering region. Comparison of the fluorescence signal, when the STIRAP method is used, with the one for FCP allows the determination of the transfer efficiency (see also [59]) because the transfer efficiency to a particular level v'', obtained with the FCP technique, is known.

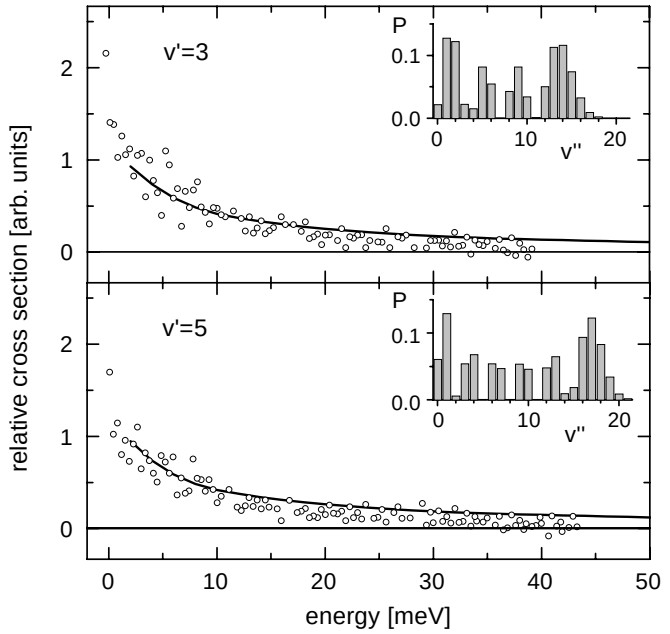

Fig. 8. Energy dependence of the relative cross-section for Na^- formation resulting from the dissociative attachment to vibrationally excited Na_2 molecules. Here, the Franck-Condon-pumping method is used, with the relative population distribution shown in the insets. The distribution is varied by exciting the different levels v' in the $A^1\Sigma_u^+$ state of the molecule.

The range of final vibrational levels, accessible by the STIRAP method from the level $v'' = 0$, is restricted by the need for strong coupling of the initial and final level with the intermediate one in order to assure adiabatic evolution during the transfer process [59–62]. With a laser power of approximately 300 mW levels in the range of $1 \leq v'' \leq 25$ can be reached.

6 Results and discussion

In this section we present the measured energy dependence of cross-sections for DA to $Na_2(v'')$ and compare the data with theoretical results.

6.1 Experimental results

Figure 8 shows results obtained by the FCP-method for vibrational excitation. The population distribution over vibrational levels in the electronic ground state is given in the inset. It depends on the level v' populated in the electronically excited state. In all cases, the rotational levels are $j'' = 9$ and 11. When the STIRAP method is used for vibrational excitation only the rotational level $j'' = 9$ is populated. At any energy, the DA cross-section decreases rapidly with decreasing v'' for $v'' < 12$ [10]. Therefore, the main contribution to the observed negative ion signal stems from levels $v'' \geq 12$. The data shown in Figure 8 characterize the overall trend: the DA cross-sections decrease monotonically with increasing electron energy. Deviation from this trend, expected for vibrational levels near the crosssing of the neutral and the ionic curve (Fig. 1), cannot be revealed using the FCP method.

The large negative ion signal for energies $\varepsilon < 0$ is due to the process of dissociative charge transfer (DCT) from high Rydberg states of the sodium atom [79]. Here, we are not concerned with this process. The solid line, shown for $\varepsilon > 0$, is the weighted sum $\sigma_{\mathrm{DA}}(v', \varepsilon) = \sum_{v''} P_{v'}(v'')\sigma_{\mathrm{DA}}(v'', \varepsilon)$, where $\sigma_{\mathrm{DA}}(v'', \varepsilon)$ are the theoretical cross-sections reported in Figure 8 of reference [10]. The overall agreement is good for these as well as for similar data based on other distributions $P_{v'}(v'')$, not shown here.

A set of data, showing the variation of the DA cross-section with electron energy for molecules which are selectively excited to vibrational levels v'' using the STIRAP method, is shown in Figure 9. All experimental data are normalized to the theoretical one by a common factor, *i.e.* the relative magnitude of the theoretical cross-section is well reproduced by the experiment. For $v'' = 22$, 14 and 13 the variation of the cross-section with energy ε agrees with the trend seen in Figure 8. However, the data for $v'' = 12$ is distinctively different. The cross-section first rises with energy to form a broad maximum around $\varepsilon = 20$ meV before it decreases again. This shape is a clear indication of a threshold for DA, which can only be revealed when individual vibrational levels are selectively populated by the STIRAP method.

6.2 Theoretical results

Our measurements corroborate quite nicely the theoretical predictions made previously [10] on the basis of *ab initio* potentials and a semi-local version of the resonance theory for the DA process, *i.e.* a local complex potential for the A state of the Na_2^- negative ion but a non-local coupling to the Na_2 (X) vibrational state in the inhomogeneous source term. The only significant deviation concerns the energy dependence in the case of $v'' = 12$ which is extremely sensitive to the small difference between the energy of this vibrational level and the energy where the potential curves cross. The proximity of these energies leads to a distinctively slower raise of the DA cross-section with decreasing electron energy than for $v'' > 12$ [10] but not in a maximum as seen in the present measurements. Pronounced maxima appeared only for $v'' < 12$ with electron energy thresholds consistent with the curve crossing close to $v'' = 12$. As stated in reference [10] this resulted from an adjustment of the A state resonance potential to match the calculated crossing, thereby also leveling off the slight maximum in the bound state part of the A potential curve between 0.4 and 0.5 nm. Such an adjustment allowed the reproduction of the large integral DA rate observed for $v'' = 12$. However, in view of the present measurements that adjustment appears to have been overdone.

Meanwhile we have recalculated the bound state potential curves using a larger basis set and an enlarged reference space built from 10 active valence orbitals in

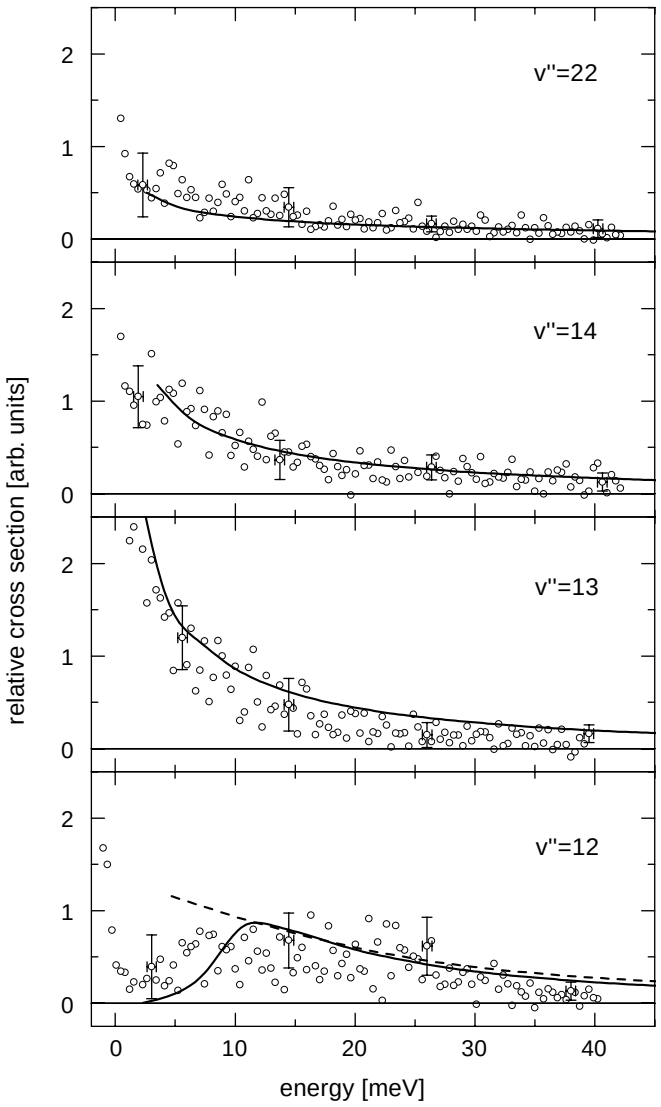

Fig. 9. Energy dependence of the relative cross-section for Na^- formation resulting from the dissociative attachment to selectively vibrationally excited Na_2 molecules. Selective excitation to the various levels v'' occurs by the STIRAP technique. All experimental data are normalized to the theoretical one by a common factor, *i.e.* the relative magnitude of the theoretical cross-section is well reproduced by the experiment. Typical error bars (based on counting statistics) are shown for a few points. The data is compared with the convoluted theoretical cross-sections based on the modified potential (solid lines). For $v'' = 12$ the results reported in reference [10] are also shown (dashed line).

a MR-CI treatment as described in reference [10]. We found a slight lowering of the Na_2^- states with respect to the Na_2 (X)-state. The electron affinity of Na_2^- (without zero-point contribution) is now 443 meV as compared to our previous value of 437 meV. The crossing region of the new potentials is shown in Figure 1. The broad maximum of the bound A-state potential is 38.5 meV above its asymptote and, for the rotational quantum number $j'' = 9$, it is 8.2 meV above the corresponding vibrational

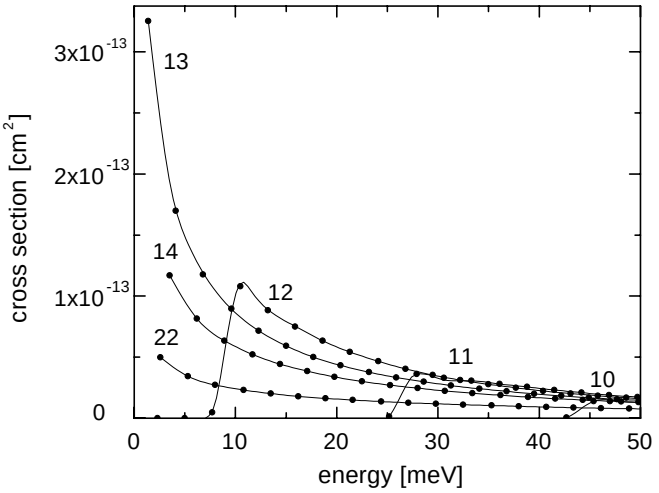

Fig. 10. Theoretical cross-section for the DA to vibrationally excited Na_2 molecules.

level $v'' = 12$. Without any adjustment we now find a steep onset of DA at 10 meV followed by a pronounced maximum (see Fig. 10). Both features are much sharper than observed. Since they are closely related to the broad maximum in the A state we do not see a good reason to attribute this discrepancy to the semi-local approximation in the treatment of the DA process.

A significantly better agreement would be achieved by convoluting the calculated cross-sections with an electron energy distribution that has a width of about 6 meV. However, we have no evidence for such a broad energy distribution in our experiment. It considerably exceeds the 2 meV estimate (based on theoretical and experimental evaluations) made above. The result of the convolution is shown in Figure 9. We note that the convolution has little effect for $v'' > 12$. There remains also a discrepancy in the case $v'' = 11$ for which the calculations predict a threshold around 30 meV. In the energy range above 35 meV the DA cross-section surpasses those for $v'' > 11$. So far, we were unable to confirm this prediction experimentally. At the present level of the signal-to-noise ratio we could not unambiguously identify a negative ion signal resulting from DA to molecules in $v'' = 11$. We assume that the cross-section for DA to molecules in $v'' = 11$ is indeed smaller than for $v'' = 12$ in this range of electron energies. Within the experimental error bars, the results of the two calculations are indistinguishable for the levels $v'' = 22$, 14, and 13. For $v'' = 12$ only the new theoretical results reproduce the indication of a maximum near $\varepsilon = 20$ meV, found in the experiment (Fig. 9). However, the experimentally observed decline of the cross-section with energy for $\varepsilon > 30$ meV, which is significantly more pronounced for $v'' = 12$ than for $v'' > 12$, is not found in either of the two calculations. A clarification of these points has probably to await a definitive determination of the resonance-to-continuum coupling which is here still modelled according to the threshold law for s-wave electron scattering as described in reference [10]. Such calculations are under way.

7 Summary and conclusion

We have presented, for the first time, a set of experimental data which reveal the energy dependence of the cross-section for dissociative attachment to molecules selectively excited to individual vibrational levels. For levels $v'' > 12$ the experimental cross-section decreases monotonically with energy, in good agreement with theoretical results. The data for $v'' = 12$ reveal the signature of the threshold expected in this region. Results from a calculation based on a modified negative ion potential reproduce the broad maximum seen in the experiment around $\varepsilon = 20$ meV but fail to agree with the experimental data for $\varepsilon > 30$ meV. For this range of energies preliminary experimental data for the level $v'' = 11$ also seems to deviate from what theory predicts. More refined experiments and calculations, which are planned, are needed to confirm or reject the speculation that this discrepancy of theory and experiment is caused by the contribution of a non-local interaction, expected to be significant for this process very close to the threshold.

This work has been supported by the Deutsche Forschungsgemeinschaft through the Forscher-gruppe "Low energy electron scattering". We thank H. Hotop for many helpful discussions.

References

1. H.S. Massey, *Negative Ions* (Cambridge University Press, 1976).
2. L.G. Christophorou, *Electron Molecule Interaction and their Applications: Volume 2* (Academic-Press, New York, 1984).
3. L. Sanche, J. Phys. B **23**, 1597 (1990).
4. A. Garscadden, Z. Phys. D **24**, 97 (1992).
5. M. Allan, S.F. Wong, Phys. Rev. Lett. **41**, 1791 (1978).
6. J.M. Wadehra, J.N. Bardsley, Phys. Rev. Lett. **41**, 1795 (1978).
7. H.L. Brooks, S.R. Hunter, K.J. Nygaard, J. Chem. Phys. **71**, 1870 (1979).
8. M. Allan, S.F. Wong, J. Chem. Phys. **74**, 1687 (1981).
9. M. Külz, A. Kortyna, M. Keil, B. Schellhaaß, K. Bergmann, Phys. Rev. A **48**, R4015 (1993).
10. M. Külz, M. Keil, A. Kortyna, B. Schellhaaß, J. Hauck, K. Bergmann, W. Meyer, D. Weyh, Phys. Rev. A **53**, 3324 (1996).
11. W.L. Fite, R.T. Brackmann, in *Proceedings of the 6th Conference on the Ionization Phenomena in Gases*, Vol. 1 (Paris, 1963).
12. W.L. Fite, R.T. Brackmann, in *Proceedings of the 4th ICPEAC* (Science Bookcrafters Inc. Hasting-on-Hudson, New York, 1965), p. 100.
13. F.K. Truby, Phys. Rev. **188**, 508 (1969).
14. W.R. Henderson, W.L. Fite, R.T. Brackmann, Phys. Rev. **183**, 157 (1969).
15. D. Spence, G.J. Schulz, J. Chem. Phys. **54**, 5424 (1971).
16. D. Teillet-Billy, J. Gauyacq, J. Phys. B **17**, 4041 (1984).
17. M.W. McGeoch, R.E. Schlier, Phys. Rev. A **33**, 1708 (1986).
18. I. Čadež, R. Hall, M. Landau, F. Pichou, C. Schermann, J. Phys. B **21**, 3271 (1988).
19. D. Popovic, I. Čadež, M. Landau, F. Pichou, C. Schermann, R.I. Hall, Meas. Sci. Technol. **1**, 1041 (1990).
20. D. Spence, G.J. Schulz, Phys. Rev. **188**, 280 (1969).
21. W.E. Wentworth, R. George, H. Keith, J. Chem. Phys. **51**, 1791 (1960).
22. P. Chantry, J. Chem. Phys. **51**, 3369 (1969).
23. F. Fehsenfeld, J. Chem. Phys. **33**, 2000 (1970).
24. B. Lehmann, Z. Naturforsch. **25**, 1755 (1970).
25. D. Spence, G. Schulz, J. Chem. Phys. **58**, 1800 (1973).
26. L.E. Kline, D.K. Davies, C.L. Chen, P.J. Chantry, J. Appl. Phys. **50**, 6789 (1979).
27. S.M. Spyrou, L.G. Christophorou, J. Chem. Phys. **82**, 2620 (1985).
28. S.M. Spyrou, L.G. Christophorou, J. Chem. Phys. **83**, 2829 (1985).
29. P. Datskos, L. Christophorou, J. Chem. Phys. **86**, 1982 (1987).
30. M. Fenzlaff, R. Gerhard, E. Illenberger, J. Chem. Phys. **88**, 149 (1988).
31. P. Datskos, L. Christophorou, J. Carter, Chem. Phys. Lett. **168**, 324 (1990).
32. P. Datskos, L. Christophorou, J. Carter, J. Chem. Phys. **97**, 9031 (1992).
33. D.M. Pearl, P.D. Burrow, I.I. Fabrikant, G.A. Gallup, J. Chem. Phys. **102**, 2737 (1995).
34. S. Matejcik, A. Kiendler, A. Stamatovic, T.D. Märk, Int. J. Mass Spectrosc. Ion Proc. **149**, 311 (1995).
35. P.D. Burrow, D.M. Pearl, Nucl. Instrum. Methods B **101**, 219 (1995).
36. F. Bruning, I. Hahndorf, A. Stamatovic, E. Illenberger, J. Phys. Chem. **100**, 19740 (1996).
37. A. Kiendler, S. Matejcik, J.D. Skalny, A. Stamatovic, T.D. Märk, J. Phys. B **29**, 6217 (1996).
38. N. Ruckhaberle, L. Lehmann, S. Matejcik, E. Illenberger, Y. Bouteiller, V. Periquet, L. Museur, C. Desfrancois, J.-P. Schermann, J. Phys. Chem. **101**, 9942 (1997).
39. I. Hahndorf, E. Illenberger, Int. J. Mass Spectrosc. Ion Proc. **167-168**, 87 (1997).
40. S. Matejcik, G. Senn, P. Scheier, A. Kiendler, A. Stamatovic, T.D. Märk, J. Chem. Phys. **107**, 8955 (1997).
41. F. Brüning, S. Matejcik, E. Illenberger, Y. Chu, G. Senn, D. Muigg, G. Denifl, T.D. Märk, Chem. Phys. Lett. **292**, 177 (1998).
42. A. Herzenberg, F. Mandl, Proc. Roy. Soc. Lond. A **270**, 48 (1962).
43. J.N. Bardsley, A. Herzenberg, F. Mandl, Proc. Phys. Soc. **89**, 321 (1966).
44. T.F. O'Malley, Phys. Rev. **150**, 14 (1966).
45. T.F. O'Malley, Phys. Rev. **155**, 69 (1967).
46. J.M. Wadehra, Appl. Phys. Lett. **35**, 917 (1979).
47. J.M. Wadehra, Phys. Rev. A **29**, 106 (1984).
48. J.N. Bardsley, J.M. Wadehra, Phys. Rev. A **20**, 1398 (1979).
49. J.M. Wadehra, Phys. Rev. A **41**, 3607 (1990).
50. A.P. Hickman, Phys. Rev. A **43**, 3495 (1991).
51. W. Domcke, C. Mündel, J. Phys. B **18**, 4491 (1985).
52. W. Domcke, H. Estrada, J. Phys. B **21**, L205 (1988).
53. W. Domcke, Phys. Rep. **208**, 97 (1991).
54. J. Horáček, W. Domcke, Phys. Rev. A **53**, 2262 (1996).

55. I.I. Fabrikant, J. Phys. B **24**, 2213 (1991).
56. J. Horáček, W. Domcke, H. Nakamura, Z. Phys. D **42**, 181 (1997).
57. L. Lehr, W. H. Miller, Chem. Phys. Lett. **250**, 515 (1996).
58. C.L. Chen, P.D. Chantry, J. Chem. Phys. **71**, 3897 (1979).
59. U. Gaubatz, P. Rudecki, S. Schiemann, K. Bergmann, J. Chem. Phys. **92**, 5363 (1990).
60. K. Bergmann, H. Theuer, B.W. Shore, Rev. Mod. Phys. **70**, 1003 (1998).
61. J.R. Kuklinski, U. Gaubatz, F.T. Hioe, K. Bergmann, Phys. Rev. A **40**, 6741 (1989).
62. K. Bergmann, B.W. Shore, *Coherent population transfer*, in *Molecular Dynamics and Spectroscopy by Stimulated Emission Pumping*, edited by H.L. Dai, R.W. Field, Adv. Phys. Chem. (World Scientific, Singapore, 1995).
63. J.-P. Ziesel, D. Teillet-Billy, L. Bouby, Chem. Phys. Lett. **123**, 371 (1986).
64. J.N. Bardsley, J.S. Cohen, Phys. Rev. B **11**, 3645 (1978).
65. J.N. Bardsley, B.R. Junker, D.W. Norcross, Chem. Phys. Lett. **37**, 502 (1976).
66. R. Shepard, K.D. Jordan, J. Simons, J. Chem. Phys. Lett. **69**, 1788 (1978).
67. K.K. Sunil, K.D. Jordan, Chem. Phys. Lett. **104**, 343 (1984).
68. J. Martin, Diploma thesis, Universität Kaiserslautern, 1991.
69. A.C. Gallagher, G. York, Rev. Sci. Ins. **45**, 662 (1974).
70. D. Field, G. Mrotzek, D.W. Knight, S. Lunt, J.P. Ziesel, J. Phys. B **21**, 171 (1988).
71. D. Field, D.W. Knight, G. Mrotzek, J. Randell, S. Lunt, J.B. Ozenne, J.P. Ziesel, Meas. Sci. Technol. **2**, 757 (1991).
72. A. Chutjian, S.H. Alajajian, Phys. Rev. A **31**, 2885 (1985).
73. A. Chutjian, *Electronic and atomic collisions*, in *Proceedings of the 17th ICPEAC*, edited by W.R. MacGillivray (Adam Hilger, Bristol, 1992).
74. D. Klar, M.-W. Ruf, H. Hotop, Meas. Sci. Technol. **5**, 1248 (1994).
75. H. Hotop, D. Klar, J. Kreil, M.-W. Ruf, A. Schramm, J.M. Weber, *Studies of low energy electron collisions at sub-meV resolution*, in *The Physics of Electronic and Atomic Collisions*, edited by L.J. Dubè, J.B.A. Mitchell, J.M. McConkey, C.E. Brion, *AIP Conference Proceedings, 19th ICPEAC, Whistler, Canada* (AIP Press, Woodbury, New York, 1995).
76. A. Schramm, J.M. Weber, J. Kreil, D. Klar, M.-W. Ruf, H. Hotop, Phys. Rev. Lett. **81**, 778 (1998).
77. U. Volz, M. Majerus, H. Liebel, A. Schmitt, H. Schmoranzer, Phys. Rev. Lett. **76**, 2862 (1996).
78. J.M. Preses, C.E. Burkhardt, R.L. Corey, D.L. Earsom, T.L. Daulton, W.P. Garver, J.J. Leventhal A.Z. Msezane, S.T. Manson, Phys. Rev. A **32**, R1264 (1985).
79. M. Keil, PhD thesis, Universität Kaiserslautern, 1998.
80. H. Hotop, Personal communication.
81. D. Klar, M.-W. Ruf, H. Hotop, Chem. Phys. Lett. **189**, 448 (1992).
82. D. Klar, B. Mirbach, H.J. Korsch, M.-W. Ruf, H. Hotop, Z. Phys. D **31**, 235 (1994).
83. C.E. Klots, Chem. Phys. Lett. **38**, 61 (1976).
84. J.P. Gauyacq, A. Herzenberg J. Phys. B **17**, 1155 (1984).
85. K. Bergmann, U. Hefter, *Spectroscopic detection methods* in *Atomic and Molecular Beam Methods*, edited by G. Scoles (Oxford University Press, 1988).
86. B. Schellhaaß, Diploma thesis, Universität Kaiserslautern, 1994.
87. M. Külz, PhD thesis, Universität Kaiserslautern, 1994.